Synthetic and Crystallographic Studies of a New Inhibitor Series Targeting *Bacillus anthracis* Dihydrofolate Reductase

Jennifer M. Beierlein,[†] Kathleen M. Frey,[†] David B. Bolstad,[†] Phillip M. Pelphrey,[†] Tammy M. Joska,[†] Adrienne E. Smith,[‡] Nigel D. Priestley,[‡] Dennis L. Wright,*[,†] and Amy C. Anderson*[,†]

Department of Pharmaceutical Sciences, University of Connecticut, 69 N. Eagleville Road, Storrs, Connecticut 06269, and Department of Chemistry, University of Montana, Missoula, Montana 59812

Received June 26, 2008

Bacillus anthracis, the causative agent of anthrax, poses a significant biodefense danger. Serious limitations in approved therapeutics and the generation of resistance have produced a compelling need for new therapeutic agents against this organism. *Bacillus anthracis* is known to be insensitive to the clinically used antifolate, trimethoprim, because of a lack of potency against the dihydrofolate reductase enzyme. Herein, we describe a novel lead series of *B. anthracis* dihydrofolate reductase inhibitors characterized by an extended trimethoprim-like scaffold. The best lead compound adds only 22 Da to the molecular weight and is 82-fold more potent than trimethoprim. An X-ray crystal structure of this lead compound bound to *B. anthracis* dihydrofolate reductase in the presence of NADPH was determined to 2.25 Å resolution. The structure reveals several features that can be exploited for further development of this lead series.

Introduction

Bacillus anthracis is the highly pathogenic, Gram-positive bacteria responsible for the acute and often fatal disease anthrax. Although known for ages as a general threat to mammals such as cattle, *B. anthracis* has more recently attracted attention as a potential bioterrorism weapon. Humans are susceptible to three forms of infection: cutaneous, gastrointestinal, and inhalational, all of which can progress to a systemic infection that ultimately proves fatal.[1] To have the greatest efficacy, the highly virulent nature of anthrax necessitates that prophylactic treatment with antibiotics is started prior to the presentation of symptoms.[2]

Fluoroquinolones, such as ciprofloxacin, are first-line therapy for anthrax, followed by doxycycline and various third-generation cephalosporins. However, each of these treatments has serious limitations: ciprofloxacin and doxycycline are expensive and are not indicated for use in children less than 8 years of age, especially as prophylactic measures without diagnosed exposure. Strains resistant to ciprofloxacin[3,4] as well as both β-lactamase-based and non-β-lactamase-based penicillin-resistant forms have emerged, and doxycyclin-resistance has been engineered in the laboratory.[2,5] The potential of a large-scale anthrax attack on a heavily populated area, with either a natural or genetically engineered resistant strain, necessitates the stockpiling of a large number of classes of low-cost and shelf-stable antibiotics. The case for the development of new classes of antibiotics against *B. anthracis* is compelling.

Dihydrofolate reductase (DHFR[a]) has been a widely recognized drug target for at least 50 years; the successful clinical use of anticancer,[6,7] antibacterial,[8,9] and antiparasitic[10] therapeutics directed against DHFR have validated this status. DHFR plays a key role in the folate biosynthesis pathway, responsible for the generation of the DNA base, deoxythymidine monophosphate, as well as the biosynthesis of purine nucleotides and the amino acids histidine and methionine. Specifically, DHFR catalyzes the reduction of dihydrofolate, using NADPH, to form tetrahydrofolate and $NADP^+$.

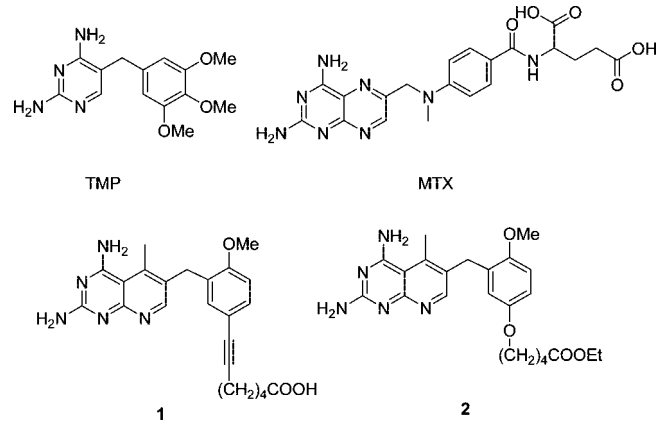

Figure 1. DHFR inhibitors trimethoprim (TMP), methotrexate (MTX) and compounds **1** and **2**.

Since human cells also depend on DHFR for DNA replication, developing inhibitors that are not only potent but also selective for the pathogen is critical. Fortunately, active site differences have allowed the development of very species-specific DHFR inhibitors for some bacteria[9] and some parasitic protozoa including *Plasmodium*[11] and *Toxoplasma.*[12] DHFR inhibitors such as methotrexate (MTX)[13] and trimethoprim (TMP) (Figure 1) have been used successfully in the clinic for several years. MTX is a potent, nonselective inhibitor employed in cancer chemotherapy, and TMP is a selective inhibitor of *E. coli* and *S. aureus* DHFR.

Previously, we[14] and others[5,15] had investigated the potential of known antifolates to be inhibitors of *B. anthracis* DHFR (BaDHFR). BaDHFR has been shown to be naturally resistant to the widely used antifolate trimethoprim but sensitive to the

* To whom correspondence should be addressed. For D.L.W.: phone, (860) 486-9451; fax, (860) 486-6857; e-mail, dennis.wright@uconn.edu. For A.C.A.: phone, (860) 486-6145; fax, (860) 486-6857; e-mail, amy.anderson@uconn.edu.

† University of Connecticut.

‡ University of Montana.

[a] Abbreviations: DHFR, dihydrofolate reductase; BaDHFR, dihydrofolate reductase from *Bacillus anthracis*; hDHFR, human dihydrofolate reductase; ChDHFR, dihydrofolate reductase from *Cryptosporidium hominis*; TMP, trimethoprim; MTX, methotrexate; NADPH, nicotinamide adenine dinucleotide phosphate, reduced form.

10.1021/jm800776a CCC: $40.75
Published on Web 11/13/2008

nonselective inhibitor methotrexate (Figure 1).[5] In addition, we examined a number of previously described antifolates[14] and discovered that extended systems such as 5-deazapteridine analogues (Figure 1; **1**, **2**) were good inhibitors of the related *B. cereus* DHFR. A recent X-ray crystal structure of BaDHFR bound to methotrexate has been reported[15] and describes differences with human DHFR as well as a potential mechanism of trimethoprim resistance.

In order to find a new class of antifolates effective against BaDHFR and selective for the bacterial enzyme, we screened a group of propargyl-based DHFR inhibitors that we have developed for pathogenic species of DHFR.[16] Using a homology model to guide the synthesis of an improved class of compounds, we synthesized a group of 2′,5′-dimethoxyphenylpyrimidines. These compounds proved to be superior in both potency and selectivity and were shown to inhibit bacterial growth. We then determined a crystal structure of the most potent and selective compound bound to BaDHFR. The crystal structure rationalizes the structure−activity relationships and provides guidance for future compound development.

Chemistry, Crystal Structure, and Biological Evaluation

Evaluation and Analysis of Existing Propargyl-Linked Inhibitors. Since anthrax is resistant to TMP and since MTX is not selective for the bacterial enzyme and hence toxic, the development of a new class of compounds is needed to effectively target the folate pathway in this organism. Interestingly, natural resistance to TMP has been noted in a wide variety of eukaryotic organisms such as the parasitic protozoa *Cryptosporidium* and *Toxoplasma* and the fungi *Candida* and *Pneumocystis.*[17] In prior work, we examined TMP resistance in *Cryptosporidium hominis* DHFR (ChDHFR). On the basis of an analysis of the structure of ChDHFR, we attributed TMP resistance to an inability of the trimethoxyphenyl ring to adequately occupy a key hydrophobic pocket in the active site of the enzyme. Subsequently, we were able to develop a highly potent and efficient lead series effective against both parasitic protozoal DHFR enzymes.[16] This novel lead series is characterized by a propargyl linker between the two arenes, providing the ideal spacing and rigidity to produce potent inhibitors. Docking representative propargyl-based compounds in a homology model of BaDHFR suggested that we could exploit a similar strategy to develop inhibitors of BaDHFR.

As we already had a number of inhibitors in hand from prior work with ChDHFR,[16] we were able to gather some preliminary structure−activity data by evaluating in vitro inhibition of BaDHFR (Table 1). We also evaluated the activity of these compounds against human DHFR in order to gauge selectivity.

Although these compounds were not highly potent inhibitors of BaDHFR, we were encouraged that most of the compounds were more potent than TMP. From this limited data set, it was apparent that certain substitutions at the propargyl position proved deleterious; substitution at the C6 position on the pyrimidine ring was tolerated. Further exploration of increased bulk at C6 and the substitution pattern on the phenyl ring was warranted.

Design, Synthesis, and Evaluation of First Generation BaDHFR Inhibitors. In an attempt to improve the potency of this series, we used structural analysis to guide the design of additional inhibitors. Since an experimental structure of BaDHFR was not available at the time, a homology model was created on the basis of the structure of the *E. coli* enzyme, which has 39% overall sequence identity and 62% identity in the active site.[14] The model was created with 3D-JIGSAW[18] and minimized using tools within Sybyl (Tripos, Inc.). Ramachandran plots of the model show that 99.4% of the residues fall within acceptable ranges (the outlier, Ile 93, is far from the active site). Comparisons of the homology model to the published crystal structure of BaDHFR show that the two models superimpose with 1.2 Å rmsd and share the same overall fold. A few residues at the opening to the active site exhibit rotamer differences. We examined the interactions of the most potent compounds, **3**−**5**, in the active site of the homology model of BaDHFR.

Table 1. Evaluation of Propargyl Inhibitors in Assays with BaDHFR and hDHFR

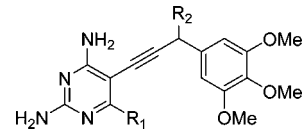

compd[a]	R_1	R_2	IC_{50} (μM) BaDHFR	IC_{50} (μM) hDHFR	selectivity ratio (h/Ba)
TMP			71	120	1.7
3	H	H	2.3	1.46	0.63
4	CH_3	H	3.7	0.4	0.11
5	H	CH_3	4.8	1.46	0.3
6	H	OH	21.2	14.3	0.67
7	H	OMe	109.2	1.16	0.01
8	CH_3	CH_3	30.3	1.38	0.05
9	CH_3	OH	14.5	5.71	0.4
10	CH_3	OMe	29.1	1.22	0.04

[a] Compounds **5**−**10** were tested as racemates.

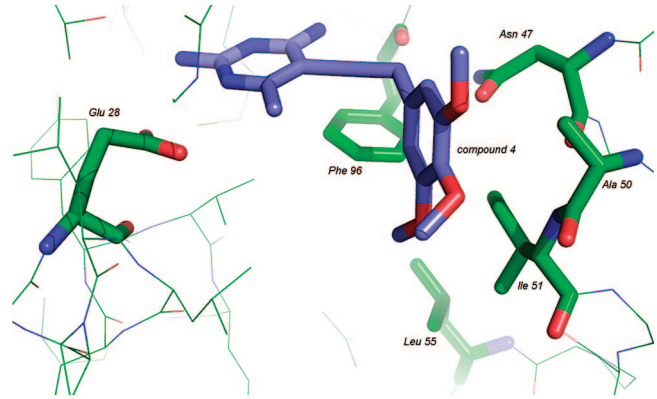

Figure 2. Homology model of BaDHFR bound to compound **4**.

The pyrimidine rings of compounds **3**−**5** appear to form the conserved interactions in the active site. This conserved orientation includes ionic interactions between the protonated N1 atom and the 2-amino group of the pyrimidine with the acidic residue Glu 28 (Figure 2).[19−22] The propargyl linker places the trimethoxyphenyl ring in van der Waals contact with the hydrophobic pocket containing Asn 47, Ala 50, Ile 51, and Leu 55. Models of **3**−**5** in the active site led us to discover that a simple change in the pattern of substitution around the phenyl ring from 3′,4′,5′-OMe to 2′,5′-OMe may maintain the interactions of the 5′-methoxy group with Leu 55 and Ile 51 while promoting a 2′ substitution to occupy the upper portion of the pocket in order to form contacts with Ala 50 and the backbone of Asn 47. Therefore, we set out to explore this alternative substitution pattern with a series of compounds that would concomitantly probe varying steric bulk at the C6 position of the pyrimidine.

For the synthesis of this propargyl-based class of inhibitors we relied on a key Sonagashira coupling to unite the arene and pyrimidine fragments, allowing a convergent, modular route.

Scheme 1[a]

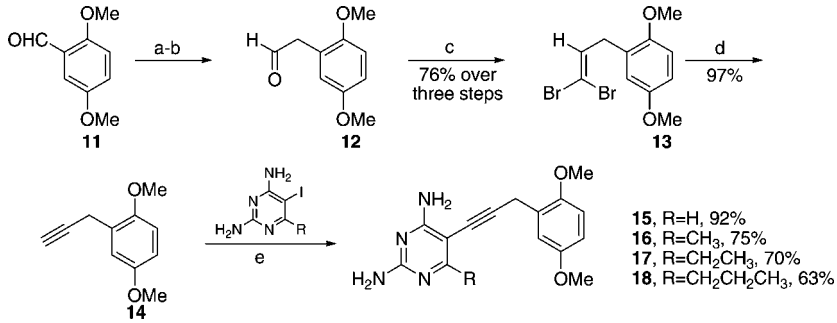

[a] (a) Ph_3PCH_2OMeCl, NaO^{t}Bu, THF, 0° C; (b) 10% HCl, THF, reflux; (c) CBr_4, PPh_3, CH_2Cl_2, 0° C; (d) Mg, THF; (e) CuI, $Pd(PPh_3)_2Cl_2$, Et_3N, DMF, 60° C.

Table 2. Inhibitory potency of first generation inhibitors

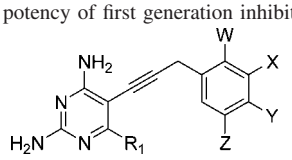

compd	R_1	W	X	Y	Z	IC$_{50}$ (μM) BaDHFR	IC$_{50}$ (μM) hDHFR	selectivity ratio
15	H	OMe	H	H	OMe	1.7	3.2	1.9
16	CH_3	OMe	H	H	OMe	1.3	1.3	1
17	Et	OMe	H	H	OMe	0.89	1.28	1.4
18	*n*-Pr	OMe	H	H	OMe	5.5	1.18	0.21
20	Et	H	OMe	OMe	OMe	0.942	0.057	0.06
22	Et	OMe	OMe	H	H	9.2	0.13	0.01
24	Et	H	H	H	H	3.2	0.36	0.11

The required propargylarenes are available through homologation of the corresponding arylaldehydes (Scheme 1).

Commercially available 2,5-dimethoxybenzaldehyde **11** was homologated to the corresponding arylacetaldehyde **12** through initial Wittig reaction to give the enol ether followed by direct hydrolysis to the aldehyde. The resulting crude material was subjected to a second homologation to give the vinyl dibromide **13** in good overall yield for the three operations. Final conversion to the terminal acetylene **14** was accomplished by a modified Corey−Fuchs reaction using elemental magnesium. Cross-coupling of **14** to four different iodinated 2,4-diaminopyrimidines[16,23,24] produced the inhibitors **15**−**18** in moderate to very good yields. The 2′,5′-dimethoxy compounds were evaluated using an in vitro enzyme inhibition assay against BaDHFR and human DHFR (Table 2).

From these assay results, it was apparent that an ethyl group at C6 was optimal. Therefore, this was maintained and three other substitution patterns on the aryl ring were explored. A trimethoxyphenyl derivative was easily prepared by coupling the previously described **19**[16] with the ethyliodopyrimidine to give **20**. A 2′3′-dimethoxy analogue **22** was prepared from commercially available 2,3-dimethoxybenzaldehyde by a route analogous to that shown in Scheme 1. Finally, a completely unsubstituted phenyl derivative **24** was synthesized in one step by coupling with commercially available phenylpropyne **23** (Scheme 2). All analogues were evaluated in enzyme inhibition assays (Table 2).

These data show that with the optimal C6-ethyl substituent, both the 2′5′-dimethoxy and the 3′,4′,5′-trimethoxy patterns are effective. However, the 2′,5′-dimethoxy pattern appears to garner a slightly favorable degree of selectivity for the bacterial enzyme. We selected four compounds, **15**−**17** and **20**, to test in an antibacterial assay against *B. anthracis* Sterne (Table 3).

Scheme 2

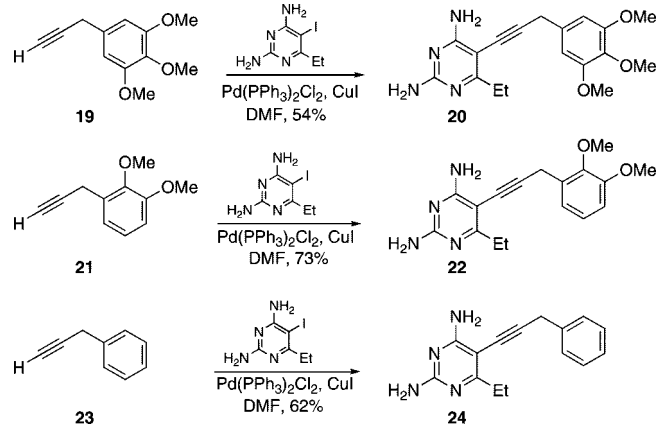

Table 3. Antibacterial Assay Results

compd	minimum inhibitory concentration (μg/mL)
15	71
16	37
17	20
20	inactive[a]

[a] Inactive at 2 mM.

We were pleased to see that these first generation inhibitors demonstrated moderate ability to kill the target organism. While growth inhibition is not at the level that would be clinically useful at this stage, the results do show that compounds in this series can function as antimicrobial agents. It is evident from these results that within the 2′,5′-dimethoxy series, as enzyme inhibition increases, antibacterial growth inhibition increases. Surprisingly, the similarly potent 3′,4′,5′-trimethoxy derivative **20** failed to inhibit bacterial growth.

X-ray Crystal Structure of BaDHFR/NADPH/Compound 17. In order to build upon these first generation compounds, we determined the crystal structure of our best lead compound, **17**, bound to BaDHFR. Crystals were grown in the presence of the cofactor NADPH as well as compound **17**, and diffraction data were collected to 2.25 Å resolution. The protein crystallized with two molecules in the asymmetric unit in space group $P4_2$. The structure was solved by molecular replacement using a previously published structure of BaDHFR bound to MTX.[15] Electron density for the ligand and cofactor was well resolved (Figure 3), allowing the construction of a model of the ternary complex. The final model is refined with an R_{free} value of 23.8 and an *R*-factor of 19.1 with all residues falling

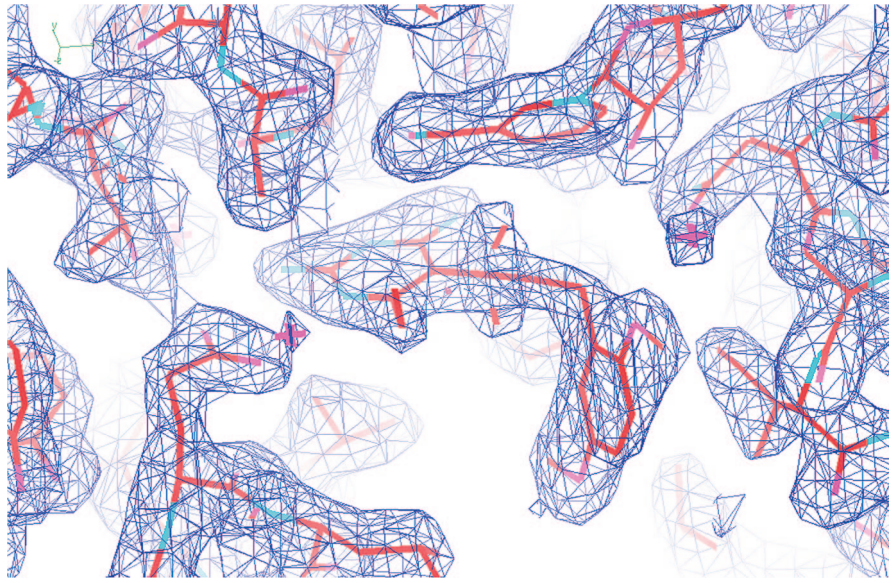

Figure 3. Electron density for the active site of the ternary complex of BaDHFR including compound **17**. Density was contoured at 2σ.

Table 4. Data Collection and Refinement Statistics for BaDHFR/**17**/NADPH

parameter	BaDHFR/**17**/NADPH
space group	$P4_2$
unit cell (a, b, c in Å)	a = 78.42, b = 78.42, c = 67.09
resolution (Å)	21.75−2.25
completeness, % (last shell*, %)	97.2 (73.6)
unique reflections	18 002
redundancy (last shell)	6.5 (6.1)
R_{sym}, % (last shell, %)	0.100 (0.299)
$\langle I/\sigma \rangle$ (last shell)	11.6 (2.2)
no. of monomers in asymmetric unit	2
Refinement Statistics	
R-factor/R_{free}	0.191, 0.238
no. of atoms (protein, ligands, solvent)	1390, 69, 127
rms deviation bond lengths (Å) angles (deg)	0.014, 1.493
average B factor (Å^2)	25.1
average B factor for ligand (Å^2)	24.5
average B factor for solvent molecules (Å^2)	29.12
Ramachandran Plot Statistics	
residues in most favored regions (%)	89.7
residues in additional allowed regions (%)	10.3
residues in generously allowed regions (%)	0.0
residues in disallowed regions (%)	0.0

into allowed regions of the Ramachandran plot (Table 4). The model has been deposited in the Protein Data Bank with code 3E0B.

The structure shows the same overall fold seen throughout several DHFR species, including a canonical eight-stranded twisted β sheet with four flanking α helices (Figure 4A). The structure of the ternary complex is similar to the published binary structure of BaDHFR bound to MTX,[15] with a root-mean-square deviation of 0.617 Å. However, there are some noticeable differences between the two structures, as observed in Figure 4B, mainly resulting from the differences in ligand and the addition of NADPH. The α helix αB, which contains residues 44−51, is positioned farther away from the inhibitor because of the proximity of the 5′-OMe group in **17**. This repositioning of αB creates additional space between itself and α helix αD, which contains residues 99−108, allowing more room for the NADPH cofactor. The βC sheet, which contains residues 60−64, is shifted to allow the residues to make polar contacts with the adenosine ring of NADPH. Distances between pairs of representative atoms on αB and βC were 1.2−1.5 Å, greater than the coordinate error of the structure (0.34 Å). Electron density was also observed for four of the six N-terminal histidines of the His-tag. Finally, there is a bulge in βA at the N-terminus, which is believed to be a result of the mutation of Ile 2 to Arg. This mutation was engineered to allow for future removal of the N-terminal His-tag. At the active site, there are only minor differences in the positions of residues, other than αB, which moves into the active site when bound to the more potent inhibitor MTX (Figure 4C).

Ligand Binding. Compound **17** is bound in the active site of BaDHFR with the pyrimidine ring demonstrating the conserved orientation for antifolate inhibitors (Figure 5). The 2-amino group forms an additional hydrogen bond with the backbone carbonyl of Val 7 and a water molecule. The carbonyl oxygen of Met 6 forms a hydrogen bond with the 4-amino group. In addition, there are several van der Waals interactions involving the pyrimidine ring and Ala 8, Val 32, Met 6, and Val 7. The ethyl group at the C6 position makes favorable lipophilic contacts with Leu 21. The acetylene linker forms van der Waals interactions with Phe 96, Leu 21, and the nicotinamide ring of NADPH. The 2′-OMe is pointed up toward a small hydrophobic pocket with Ala 50 and Leu 21, while the 5′-OMe is pointed down toward a larger hydrophobic pocket comprising Ile 51, Leu 55, Leu 29, and Phe 96. An ordered water molecule in the active site forms hydrogen bonds to Glu 28 and Trp 23 and has been observed in other species of DHFR.[21] A second water molecule forms hydrogen bonds to the 2′-OMe on the phenyl ring.

The structural analysis rationalizes some of the trends observed in the preliminary compound evaluation. The C6 ethyl substitution appears to be optimal because the terminal methyl group is properly situated to form favorable interactions with Leu 21. This interaction is not possible with hydrogen or methyl at C6, while the larger propyl group likely introduces destabilizing interactions. The acetylenic linker seems ideally suited to bypass the restricted space introduced by Phe 96 and position the aryl ring in the hydrophobic pocket. Furthermore, the deleterious effect of propargylic substitution is rationalized by destabilizing interactions with either Phe 96 or the nicotinamide ring of NADPH. Finally, it appears that the 2′-OMe anchors the phenyl ring by binding the small hydrophobic pocket, allowing the 5′-OMe to explore the larger pocket below.

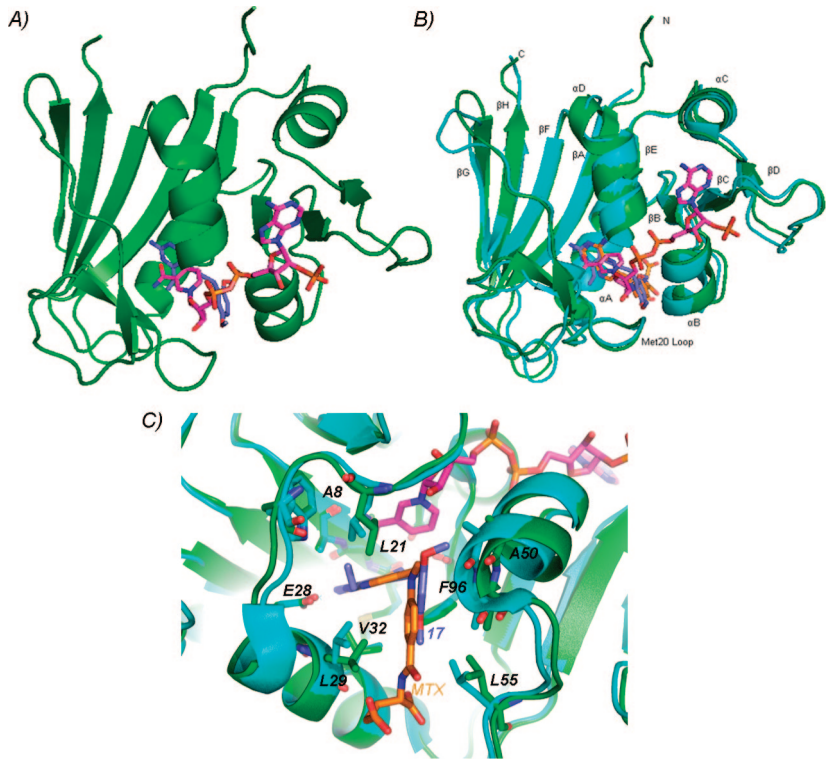

Figure 4. (A) overall structure of BaDHFR bound to NADPH and **17** and a comparison with (B) overall binary complex with MTX (PDB 2QK8[15]) and (C) residues and ligands at the active site.

Substituents at the 3′ position are not likely to make any productive contacts, while groups at the 4′ position may have an opportunity to interact with Leu 29.

In summary, we have identified a novel, flexible lead series effective as inhibitors of the enzyme BaDHFR as well as the growth of *B. anthracis* Sterne. The best compound in this series makes several key interactions with the active site of BaDHFR, which results in a greater than 88-fold increase in potency relative to trimethoprim. Further development of this class will necessitate both an increase in potency against BaDHFR and an increase in selectivity over the human form of the enzyme. Improvements in potency and selectivity, while maintaining good druglike properties, should lead to a corresponding increase in antibacterial activity. Analysis of the experimentally determined structure of BaDHFR bound to compound **17** reveals several design strategies for superior analogues.

A structure-based sequence alignment and structural comparison (Figure 6) show that there are several residue differences between BaDHFR and hDHFR, providing opportunities to garner selectivity in future designs. Specifically, optimization of the substituent at the C6 position of the pyrimidine ring may lead to increased potency and selectivity. Branching at the arylic position at C6, such as isopropyl, cyclopropyl, or *tert*-butyl, would be expected to project functionality into the larger hydrophobic pocket below the pyrimidine ring comprising Val 32 and Leu 29 in BaDHFR. The structural comparison with hDHFR shows that the corresponding residues are both larger (Phe 31 and Phe 34) in the human enzyme. Therefore, the potential exists for destabilizing interactions with these branched substituents at the C6 position, which could lead to an increase in selectivity. Alternatively, increased bulk at the 5′ position of the aryl ring could form additional hydrophobic interactions with the larger pocket comprising Ile 51, Leu 55, Leu 29, and Phe 96 (Figure 7). Again, the phenylalanine residues in hDHFR restrict the volume of this pocket and as such present an opportunity for increasing selectivity. Additionally, increased bulk at the 5′ position may result in destabilizing interactions with a loop at the active site (Pro 61−Glu 62−Lys 63−Asn 64, the PEKN loop) in hDHFR that is absent in BaDHFR. Finally, substitution at the 4′ position of the aryl ring could interact with Leu 29, yielding an increase in potency. Current work is focused on the design and synthesis of second generation inhibitors of BaDHFR.

Experimental Section

Enzyme Cloning. Site-directed mutagenesis was used to change the earlier reported construct for BcDHFR-pET41[14] to BaDHFR by three point mutations: V77A, I130M, and I138V. Mutations were verified by ABI Big Dye sequencing. The BaDHFR-pET41 construct was amplified using PCR and inserted into vector pQE2. BaDHFR-pQE2 clones were verified by sequencing. The resulting construct contained the BaDHFR gene with an N-terminus histidine tag and a DAPase stop point (Ile 2 was mutated to Arg) for future His-tag removal.

Genomic DNA containing the gene for hDHFR was obtained from ATCC and amplified by PCR. The gene was inserted into the pET41 vector and verified by sequencing. Expression and purification methods described for BcDHFR-pET41[14] were followed for hDHFR.

Recombinant Protein Expression and Purification. BaDHFR recombinant protein was expressed in M15 cells upon induction with 1 mM IPTG at mid-log phase. Protein expression was extended for an additional 6 h at 37 °C after induction. Cells were harvested by centrifugation. Pellets were lysed with 1× Bugbuster and DNase for 20 min at room temperature and then centrifuged at high speed to collect the supernatant. The supernatant was loaded onto a nickel affinity column and washed with 20 mM Tris, 1 mM DTT, 200 mM KCl (pH 8.0). Bound protein was eluted across a linear gradient with 20 mM Tris, pH 8.0, 1 mM DTT, 50 mM KCl, and 250 mM imidazole. The fractions with pure protein were concentrated to ∼1 mL and loaded onto a size exclusion column (S200) for desalting. Protein was eluted into a final buffer of 20 mM Tris, 50

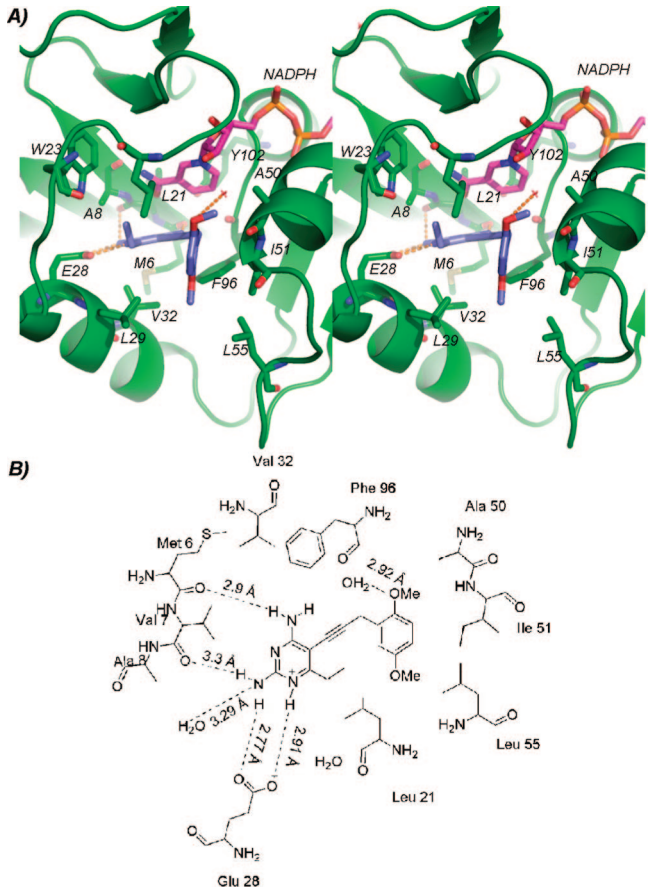

Figure 5. Detailed interactions of the ligand with the active site residues. (A) Stereoview of the active site with NADPH in magenta and compound **17** in blue. Water molecules are shown as "x", and orange dashed lines indicate hydrogen bonds. (B) Two-dimensional depiction of protein−ligand interactions. Hydrogen bonds are noted with dashed lines and distance measurements.

mM KCl, 5 mM DTT, and 0.5 mM EDTA. Fractions were analyzed by SDS−PAGE. Protein was concentrated to ∼5 mg/mL and stored at −20 °C until crystal tray setup.

Enzyme Assays. Enzyme activity assays were performed at 25 °C by monitoring the rate of enzyme-dependent NADPH oxidation at an absorbance of 340 nm over several minutes.[14] Reactions were performed in a buffer containing 20 mM TES, pH 7.0, 50 mM KCl, 10 mM 2-mercaptoethanol, 0.5 mM EDTA, and 1 mg/mL BSA. All enzyme assays were performed with a single, limiting concentration of enzyme and saturating concentrations of NADPH and dihydrofolate. IC_{50} values were calculated as the average of three independent experiments.

Antibacterial Assays. Minimum inhibitory concentrations (MIC) against *B. anthracis* Sterne were determined using a broth microdilution approach based upon CLSI (formerly NCCLS) standards and the use of the colorimetric reporter Alamar Blue. The MIC value is the lowest concentration of test compound that inhibits growth such that less than 1% reduction of the blue resazurin (ν_{max} = 570 nm) component of the Alamar Blue to the pink resorufin (ν_{max} = 600 nm) is observed.

Crystallization. Protein at 5 mg/mL concentration was incubated with 2 mM NADPH and 1 mM compound **17** for 1 h at 4 °C. After incubation, the protein−ligand mix was concentrated to 15 mg/mL using a microcon (Amicon). All crystallization trials were conducted at 25 °C. Initial hits were grown by hanging-drop vapor diffusion in 25% (w/v) PEG 10,000, 0.1 M MES, pH 6.5, at an equal ratio of protein to crystallization solution. Microseeding was used to obtain isolated crystals in 10% (w/v) PEG 10,000 and 0.1 M MES, pH 6.5, at a protein concentration of 10 mg/mL. Good quality crystals were cryoprotected in 15% ethylene glycol and flash-cooled with liquid nitrogen. Data were collected at Brookhaven National Synchotron Light Source on beamline X29A. All data sets were collected at 100 K.

Structure Determination. The structure of the BaDHFR−ligand complex was solved by molecular replacement. The program Phaser and a published model of BaDHFR (PDB code 2QK8[15]) were used to determine initial phase information. The program Coot was used to visualize the electron density map and build the model. The model was refined with the program Refmac5. The refined model satisfies the conditions of the Ramachandran plot (Table 2).

Synthesis: General. The ^1H and ^{13}C spectra were recorded on Bruker instruments at 500 and 125 MHz or 300 and 75 MHz, respectively. Melting points were recorded on Mel-Temp 3.0 apparatus and are uncorrected. High-resolution mass spectrometry was provided by the Washington University Mass Spectrometry Laboratory or the Notre Dame Mass Spectrometry Laboratory. IR data were obtained a Shimadzu 8400-s FTIR spectrometer. Anhydrous dichloromethane, ether, and tetrahydrofuran were used directly from Baker cycletainers. Anhydrous dimethylformamide was purchased from Acros and degassed by purging with argon. Anhydrous triethylamine was purchased from Aldrich and degassed by purging with argon. TLC analyses were performed on Whatman Partisil K6F silica gel 60 plates and visualized at 254 nm and/or by staining with potassium permanganate. All reagents were used directly from commercial sources unless otherwise stated. All glassware was oven-dried and allowed to cool under an argon atmosphere. Compounds **3**−**10** were previously synthesized according to literature procedures.[16] 2,4-Diamino-5-iodopyrimidine,[16] 2,4-diamino-5-iodo-6-methylpyrimidine,[16] 2,4-diamino-6-ethyl-5-iodopyrimidine,[23] and 2,4-diamino-6-*n*-propylpyrimidine[24] were synthesized according to literature procedures.

1,1-Dibromo-3-(2,5-dimethoxyphenyl)propene (13). To a 0 °C suspension of methoxymethyltriphenylphosphonium chloride (10.8 g, 31.6 mmol) in dry THF (90 mL) under an argon atmosphere is added NaO^{t}Bu (3.90 g, 40.6 mmol) in one portion. The red-orange suspension is stirred for a further 10 min at 0 °C, and then solid 2,5-dimethoxybenzaldehyde **11** (3.0 g, 18.1 mmol) was added in small portions. After 10 min, the reaction was quenched with water (50 mL) and diluted with ether (50 mL). The organic phase was separated and the aqueous phase extracted with additional ether (2 × 50 mL). The combined organics were washed with brine (50 mL), dried over sodium sulfate, and concentrated to afford the crude product that was filtered through a column of silica (SiO_2 75 g, 5% EtOAc/hexanes) to afford the crude enol ether that was immediately hydrolyzed in the subsequent step.

To a solution of crude enol ether in THF (110 mL) was added 10% aqueous HCl (10 mL). The solution was heated to refllux and monitored by TLC. The reaction was proceeding sluggishly after 1 h, so an additional 0.5 mL of concentrated HCl was added. Once the starting material had been consumed (∼1 h), the reaction mixture was diluted with saturated $NaHCO_3$ (100 mL). THF was removed at the rotovap, and the aqueous mixture was extracted with ether (3 × 50 mL). The combined organics were washed with brine (2 × 50 mL), dried over sodium sulfate, and concentrated to afford the crude aldehyde **12** (3.02 g, 93%, two steps) that was taken immediately to the next step. TLC R_f = 0.31 (15% EtOAc/hexanes); ^1H NMR (300 MHz, $CDCl_3$) δ 9.67 (t, J = 2.1 Hz, 1H), 6.83 (m, 2H), 6.73 (m, 1H), 3.78 (s, 3H), 3.77 (s, 3H), 3.62 (d, J = 2.1 Hz, 2H).

To a 0 °C solution of CBr_4 (8.36 g, 25.2 mmol) in dry CH_2Cl_2 (100 mL) was added PPh_3 (13.20 g, 50.3 mmol) in a single portion. The resulting dark-yellow solution was stirred a further 5 min, and then crude aldehyde **12** dissolved in CH_2Cl_2 (10 mL) was added dropwise. The solution was stirred for 30 min and then poured into ice cold ether (450 mL), producing a white precipitate and yellow oil. The mixture was filtered through a column of silica gel (100 g) equilibrated with hexanes, and rinsed with hexanes (100 mL) and 15% EtOAc/hexanes (300 mL). The filtrate was concentrated and the residue purified by flash chromatography (SiO_2 100 g, 10% EtOAc/hexanes) to afford dibromoalkene **13** as a clear viscous oil

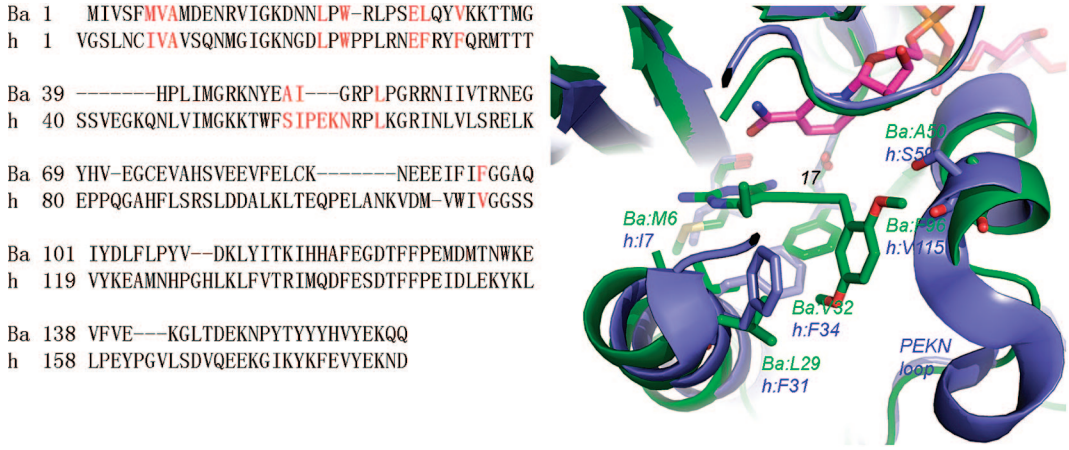

Figure 6. Structural alignment of BaDHFR and hDHFR: (left) structure-based sequence alignment, where residues in the active site are shown in red; (right) superposition of BaDHFR (green) and hDHFR (purple) with active site residue substitutions labeled.

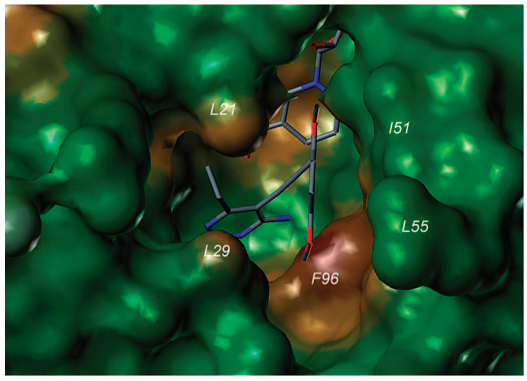

Figure 7. Surface depiction of binding pocket surrounding compound **17**. The surface is colored with a lipophilicity gradient. Compound **17** and NADPH are shown as gray sticks with atom colors. Figure was generated by Sybyl 8.0.

(4.63 g, 76% from **11**, three steps). TLC $R_f = 0.61$ (15% EtOAc/hexanes); ^{1}H NMR (300 MHz, $CDCl_3$) δ 6.81−6.71 (m, 3H), 6.57 (t, $J = 7.3$ Hz, 1H), 3.80 (s, 3H), 3.77 (s, 3H), 3.39 (d, $J = 7.3$ Hz, 2H); ^{13}C NMR (75 MHz, $CDCl_3$) δ 153.6, 151.5, 136.7, 127.0, 116.3, 111.9, 111.3, 89.5, 55.9, 55.7, 34.1; IR (neat, KBr, cm^{-1}) 2949, 2831, 1591, 1504, 1227, 1045, 787; HRMS (FAB, M^+) *m/z* 333.9188 (calculated for $C_{11}H_{12}Br_2O_2$, 333.9204).

3-(2,5-Dimethoxyphenyl)propyne (14). To the dibromoalkene **13** (0.313 g, 0.93 mmol) in an 8 mL screw-cap vial was added magnesium (0.045 g, 1.88 mmol) and dry THF (1 mL). The vial was flushed with argon and sealed tightly with a rubber septum. The mixture was heated in a 75 °C oil bath for 15 min when a check by TLC showed consumption of the starting material. The mixture was cooled and the residue purified by flash chromatography (SiO_2 17 g, 10% EtOAc/hexanes) to afford acetylene **14** as a clear viscous oil (0.160 g, 97%): TLC $R_f = 0.39$ (5% EtOAc/hexanes); ^{1}H NMR (300 MHz, $CDCl_3$) δ 7.15 (m, 1H), 6.80−6.72 (m, 2H), 3.800 (s, 3H), 3.797 (s, 3H), 3.58 (d, $J = 2.7$ Hz, 2H), 2.20 (t, $J = 2.7$ Hz, 1H); ^{13}C NMR (75 MHz, $CDCl_3$) δ 153.6, 150.9, 125.6, 115.3, 111.9, 110.9, 81.7, 70.5, 55.8, 55.6, 19.3; IR (neat, KBr, cm^{-1}) 3290, 2999, 2833, 1593, 1499, 1220, 1049; HRFAB [MLi^+] 183.1000 (calculated for $C_{11}H_{12}O_2Li$, 183.0997).

2,4-Diamino-5-[3-(2,5-dimethoxyphenyl)prop-1-ynyl]pyrimidine (15). To an oven-dried 8 mL screw-cap vial was added 2,4-diamino-5-iodopyrimidine (0.145 g, 0.614 mmol), CuI (18 mg, 0.094 mmol, ~15%), and $Pd(PPh_3)_2Cl_2$ (30 mg, 0.043 mmol, ~7%). Degassed (argon purge) anhydrous DMF (1.5 mL) was added followed by alkyne **14** (0.271 g, 1.54 mmol) as a solution in DMF (1 mL). Degassed (argon purge) anhydrous triethylamine was added (2.5 mL), and the mixture was degassed once using the freeze−pump−thaw method. The vial was sealed under argon and heated at 50 °C for 1 h. After cooling, the orange solution was diluted with EtOAc (60 mL) and washed with a water/saturated $NaHCO_3$ solution (1:2, 30 mL × 3) and brine (2 × 30 mL). The organic phase was dried over sodium sulfate and concentrated to afford the crude product that was purified by flash chromatography (SiO_2 15 g, EtOAc) to provide the coupled pyrimidine **15** as a pale solid (0.144 g, 92%). An analytical sample was generated by triturating under DCM. TLC $R_f = 0.61$ (9:1, $CHCl_3$/MeOH); mp, decomposed above 180 °C; ^{1}H NMR (500 MHz, DMSO-d_6) δ 7.88 (vbs, 1H), 7.05 (d, $J = 3.1$ Hz, 1H), 6.91 (d, $J = 8.9$ Hz, 1H), 6.79 (dd, $J = 8.9, 3.1$ Hz, 1H), 6.41 (vbs, 2H), 6.22 (s, 2H), 3.76 (s, 3H), 3.73 (s, 2H), 3.70 (s, 3H); ^{13}C NMR (125 MHz, DMSO-d_6) δ 163.8, 162.0, 158.5, 153.1, 150.6, 126.0, 115.3, 111.7, 111.5, 92.6, 90.5, 76.4, 55.8, 55.3, 20.2; HRFAB [MLi^+] 291.1442 (calculated for $C_{15}H_{16}N_4O_2Lim$ 291.1433); HPLC (a) $t_R = 4.71$ min, 100%, (b) $t_R = 8.27$ min, 98.8%. Anal. ($C_{15}H_{16}N_4O_2$) C, H, N.

2,4-Diamino-5-[3-(2,5-dimethoxyphenyl)prop-1-ynyl]-6-methylpyrimidine (16). To an oven-dried 8 mL screw-cap vial was added 2,4-diamino-5-iodo-6-methylpyrimidine (0.162 g, 0.648 mmol), CuI (18 mg, 0.094 mmol, ~15%), and $Pd(PPh_3)_2Cl_2$ (32 mg, 0.046 mmol, ~7%). Degassed (argon purge) anhydrous DMF (1.5 mL) was added followed by alkyne **14** (0.285 g, 1.62 mmol) as a solution in DMF (1 mL). Degassed (argon purge) anhydrous triethylamine was added (2.5 mL), and the mixture was degassed once using the freeze−pump−thaw method. The vial was sealed under argon and heated at 50 °C for 2 h. After cooling, the orange solution was diluted with EtOAc (50 mL) and washed twice with a water/saturated $NaHCO_3$ solution (1:2, 30 mL) and then brine (30 mL). The organic phase was dried over sodium sulfate and concentrated to afford the crude product that was purified by flash chromatography (SiO_2 14 g, EtOAc) to provide coupled pyrimidine **16** (0.145 g, 75%) as a white powder. $R_f = 0.61$ (9:1, $CHCl_3$/MeOH); mp, decomposed above 180 °C; ^{1}H NMR (500 MHz, DMSO-d_6) δ 7.07 (d, $J = 3.1$ Hz, 1H), 6.92 (d, $J = 8.9$ Hz, 1H), 6.79 (dd, $J = 8.9, 3.1$ Hz, 1H), 6.28 (vbs, 2H), 6.13 (s, 2H), 3.77−3.76 (m, 5H), 3.70 (s, 3H), 2.20 (s, 3H); ^{13}C NMR (125 MHz, DMSO-d_6) δ 166.8, 164.3, 160.9, 153.1, 150.6, 126.2, 115.0, 111.8, 111.5, 95.4, 88.7, 76.5, 55.8, 55.3, 22.4, 20.5; HRFAB [MLi^+] 305.1591 (calculated for $C_{16}H_{18}N_4O_2Li$, 305.1590); HPLC (a) $t_R = 5.33$ min, 98.6%, (b) $t_R = 8.92$ min, 99.1%.

2,4-Diamino-5-[3-(2,5-dimethoxyphenyl)prop-1-ynyl]-6-ethylpyrimidine (17). To an oven-dried 15 mL sealed tube was added 2,4-diamino-6-ethyl-5-iodopyrimidine (0.132 g, 0.50 mmol), $Pd(PPh_3)_2Cl_2$ (24.6 mg, 0.035 mmol, 7% Pd), CuI (6.6 mg, 0.035 mmol, 7%), and acetylene **14** (0.176 g, 1.00 mmol). Degassed (argon purge) anhydrous DMF and triethylamine (2.5 mL each) were added, and the tube was sealed and the mixture degassed by one cycle of freeze−pump−thaw. The mixture was stirred at 50 °C for 15 h and then added to a separatory funnel containing EtOAc

(20 mL). The organic layer was washed twice with a water/saturated $NaHCO_3$ solution (1:2, 8 mL) and then brine (8 mL). The organic layer was then dried over $MgSO_4$ and concentrated under reduced pressure. The residue was purified by flash chromatography (SiO_2, 40 g, 1% MeOH in $CHCl_3$) to afford coupled product **17** as a white powder (0.110 g, 70%). An analytical sample was obtained by crystallization from MeCN. TLC $R_f = 0.61$ (9:1, $CHCl_3$/MeOH); mp, decomposed above 180 °C; ^{1}H NMR (500 MHz, DMSO-d_6) δ 7.06 (d, $J = 2.9$ Hz, 1H), 6.91 (d, $J = 8.8$ Hz, 1H), 6.79 (dd, $J = 8.8$, 2.9 Hz, 1H), 6.18 (s, 2H), 3.77−3.76 (m, 5H), 3.70 (s, 3H), 2.54 (q, $J = 7.6$ Hz, 2H), 1.12 (t, $J = 7.6$ Hz, 3H); ^{13}C NMR (125 MHz, DMSO-d_6) δ 171.5, 164.5, 161.2, 153.1, 150.6, 126.3, 115.0, 111.8, 111.4, 95.2, 87.9, 76.2, 55.8, 55.3, 28.9, 20.6, 12.6; HRFAB [MLi^+] 319.1736 (calculated for $C_{17}H_{20}N_4O_2Li$, 319.1746); HPLC (a) $t_R = 6.13$ min, 96.0%, (b) $t_R = 8.85$ min, 97.0%.

2,4-Diamino-5-iodo-6-*n*-propylpyrimidine. To a flame-dried 200 mL flask was added 2,4-diamino-6-*n*-propylpyrimidine (3.0 g, 0.016 mol) in MeOH (56 mL) followed by dropwise addition of 1.0 M ICl solution in CH_2Cl_2 (56 mL, 0.056 mol). The solution was stirred at 25 °C for 18 h and then the solvent removed under reduced pressure. The resulting viscous oil was stirred in Et_2O (150 mL) for 2 h. The resulting solid was filtered off and washed with Et_2O (3 × 10 mL) to afford the HCl salt as a yellow solid. The crude salt was suspended in 1.0 N NaOH (150 mL) and stirred at 25 °C for 2 h. The solid was filtered, washed with cold water (2 × 10 mL) followed by cold Et_2O (3 × 10 mL), and dried under vacuum to afford the product as a brown powder (1.86 g, 41.5%). An analytical sample was prepared by recrystallization from MeCN to give title compound as colorless crystals. $R_f = 0.63$ (9:1, $CHCl_3$/MeOH); mp, 187.0−188.5 °C; ^{1}H NMR (500 MHz, DMSO-d_6) δ 6.32 (bs, 2H), 6.03 (bs, 2H), 2.53 (t, $J = 7.5$ Hz, 2H), 1.58 (sextet, $J = 7.5$ Hz, 2H), 0.93 (t, $J = 7.5$ Hz, 3H); ^{13}C NMR (125 MHz, DMSO-d_6) δ 170.1, 163.6, 163.0, 64.5, 42.7, 21.6, 14.4; HRMS (FAB, MH^+) m/z 279.0106 (calculated for $C_7H_{12}IN_4$, 279.0107).

2,4-Diamino-5-[3-(2,5-dimethoxyphenyl)prop-1-ynyl]-6-*n*-propylpyrimidine (18). To an oven-dried 8 mL vial was added 2,4-diamino-5-iodo-6-*n*-propylpyrimidine (0.1202 g, 0.43 mmol), $Pd(PPh_3)_2Cl_2$ (34 mg, 0.043 mmol, 10% Pd), CuI (18 mg, 0.095 mmol, 22%). Degassed (argon purge) anhydrous DMF (0.75 mL) and triethylamine (1.25 mL) were added, followed by acetylene **14** (0.156 g, 0.86 mmol) in DMF (0.50 mL). The vial was sealed and the mixture degassed by one cycle of freeze−pump−thaw. The mixture was stirred at 60 °C for 17 h. The reaction mixture was then added to a separatory funnel containing EtOAc (20 mL). The organic layer was washed twice with a water/saturated $NaHCO_3$ solution (1:2, 20 mL) and then brine (20 mL). The organic layer was then dried over $MgSO_4$ and concentrated under reduced pressure. The residue was preloaded onto silica gel and purified by flash chromatography (SiO_2, 15 g), eluting with straight EtOAc to afford the coupled pyrimidine **18** as a pale-yellow powder (0.0889 g, 63%). An analytical sample was obtained by crystallization from MeCN. TLC $R_f = 0.63$ (9:1 $CHCl_3$/MeOH); mp, decomposed above 158.5 °C; ^{1}H NMR (500 MHz, $CDCl_3$) δ 7.12 (m, 1 H), 6.82 (d, $J = 5.0$ Hz, 1H), 6.80 (m, 1H), 5.16 (bs, 2H), 4.76 (bs, 2H), 3.85 (s, 5H), 3.80 (s, 3H), 2.68 (t, $J = 5.9$ Hz, 2H), 1.73 (sextet, $J = 5.9$ Hz, 2H), 0.99 (t, $J = 5.9$ Hz, 3H); ^{13}C NMR (125 mHz, $CDCl_3$) δ 172.1, 164.4, 160.5, 153.7, 151.1, 126.5, 115.4, 112.0, 111.1, 96.2, 91.4, 75.4, 55.9, 55.7, 38.3, 21.88, 21.0, 14.1; HRMS (FAB, MH^+) m/z 327.1826 (calculated for $C_{18}H_{23}N_4O_2$, 327.1821); HPLC (a) $t_R = 7.19$ min, 98.2%, (b) $t_R = 9.93$ min, 99.0%.

2,4-Diamino-5-[3-(3,4,5-trimethoxyphenyl)prop-1-ynyl]-6-ethylpyrimidine (20). To an oven-dried 8 mL screw-cap vial was added alkyne **19** (0.190 g, 0.921 mmol), 2,4-diamino-6-ethyl-5-iodopyrimidine (0.122 g, 0.462 mmol), CuI (0.015 g, 0.079 mmol, ∼17%), and $Pd(PPh_3)_2Cl_2$ (23 mg, 0.033 mmol, ∼7%). Degassed (argon purge) anhydrous DMF and degassed anhydrous triethylamine were added (1.25 mL each), and the mixture was degassed once using the freeze−pump−thaw method. The vial was sealed under argon and heated at 60 °C for 4 h. After cooling, the orange solution was diluted with EtOAc (20 mL) and washed twice with a water/saturated $NaHCO_3$ solution (1:2, 20 mL) and brine (20 mL). The organic phase was dried over sodium sulfate and concentrated to afford the crude product that was purified by flash chromatography (SiO_2 13 g, EtOAc) to afford coupled pyrimidine **20** as a tan powder (0.086 g, 54%). TLC $R_f = 0.22$ (EtOAc); mp 176 − 178 °C; ^{1}H NMR (500 MHz, DMSO-d_6) δ 6.71 (s, 2H), 6.30 (vbs, 2H), 6.15 (bs, 2H), 3.85 (s, 2H), 3.77 (s, 6H), 3.64 (s, 3H), 2.56 (q, $J = 7.5$ Hz, 2H), 1.12 (t, $J = 7.5$ Hz, 3H); ^{13}C NMR (125 MHz, DMSO-d_6) δ 171.5, 164.4, 161.2, 152.8, 136.0, 133.0, 105.0, 95.7, 87.9, 76.2, 60.0, 55.7, 28.8, 25.7, 12.5; HRMS (FAB, MH^+) m/z 343.1784 (calculated for $C_{18}H_{23}N_4O_3$, 343.1770); HPLC (a) $t_R = 4.21$ min, 99.3%, (b) $t_R = 8.27$ min, 98.7%. Anal. ($C_{18}H_{22}N_4O_3$) C, H, N.

3-(2,3-Dimethoxyphenyl)propyne (21). To a 0 °C suspension of methoxymethyltriphenylphosphonium chloride (1.80 g, 5.25 mmol) in dry THF (15 mL) under an argon atmosphere is added NaO^{t}Bu (0.65 g, 6.76 mmol) in one portion. The red-orange suspension was stirred for a further 3 min at 0 °C, and then 2,3-dimethoxybenzaldehyde (0.50 g, 3.0 mmol) was added directly in small portions. After 5 min, the reaction was quenched with water (15 mL) and allowed to stir for 16 h (can be worked up immediately). The mixture was diluted with ether (15 mL), and the organic phase was separated. The aqueous phase was extracted with additional ether (2 × 10 mL) and the combined organics were washed with brine (15 mL), dried over sodium sulfate, and concentrated to afford the crude product that was filtered through a column of silica (SiO_2 19 g, 5% EtOAc/hexanes) to afford the crude enol that was immediately hydrolyzed in the subsequent step. TLC $R_f = 0.36$ (15% EtOAc/hexanes).

To a solution of crude enol ether in THF (13 mL) was added 10% aqueous HCl (3 mL). The solution was heated to reflux and monitored by TLC. Once the starting material had been consumed (∼1.5 h), the mixture was cooled and diluted with saturated $NaHCO_3$ and ether (15 mL each). The organic phase was separated and the aqueous phase extracted with additional ether (2 × 15 mL). The combined organics were washed with saturated $NaHCO_3$ (20 mL) and brine (20 mL), dried over sodium sulfate, and concentrated to afford the crude product that was used directly in the next step. TLC $R_f = 0.30$ (15% EtOAc/hexanes).

To a 0 °C solution of CBr_4 (2.61 g, 7.87 mmol) in dry CH_2Cl_2 (45 mL) was added PPh_3 (4.11 g, 15.7 mmol) in a single portion. The resulting dark-yellow solution was stirred a further 5 min, and then the crude aldehyde dissolved in CH_2Cl_2 (3.5 mL) was added dropwise. The resulting solution was stirred for 30 min and then poured into ice cold ether (250 mL), producing a white precipitate. The mixture was filtered through a column of silica gel (37 g) equilibrated with hexanes and rinsed with 15% EtOAc/hexanes until product elution ceased. The filtrate was concentrated and the residue purified by flash chromatography (SiO_2 23 g, 5−10% EtOAc/hexanes) to afford 1,1-dibromo-3-(2,3-dimethoxyphenyl)propene as a clear, viscous oil (0.752 g, 74%, three steps). TLC $R_f = 0.46$ (15% EtOAc/hexanes); ^{1}H NMR (500 MHz, $CDCl_3$) δ 7.01 (at, $J = 8.0$ Hz, 1H), 6.83 (dd, $J = 8.2$, 1.3 Hz, 1H), 6.79 (dd, $J = 7.7$, 1.3 Hz, 1H), 6.55 (t, $J = 7.2$ Hz, 1H), 3.87 (s, 3H), 3.84 (s, 3H), 3.45 (d, $J = 7.2$ Hz, 2H); ^{13}C NMR (125 MHz, $CDCl_3$) δ 152.8, 146.9, 137.0, 131.4, 124.1, 121.6, 111.0, 89.5, 60.6, 55.7, 33.7; IR (neat, KBr, cm^{-1}) 2997, 2935, 2833, 1585, 1481, 1275, 1080, 789; HRMS (FAB, M^+) m/z 333.9189 (calculated for $C_{11}H_{12}Br_2O_2$, 333.9204).

To the dibromoalkene (0.530 g, 1.58 mmol) in an 8 mL screw-cap vial was added magnesium (0.078 g, 3.25 mmol) and dry THF (1.5 mL). The vial was flushed with argon and sealed tightly with a rubber septum. The mixture was heated in a 75 °C oil bath for 40 min when a check by TLC showed consumption of the starting material. The mixture was cooled and the residue purified by flash chromatography (SiO_2 22 g, 10% EtOAc/hexanes) to afford acetylene **21** as a clear viscous oil (0.252 g, 91%). TLC $R_f = 0.39$ (5% EtOAc/hexanes); ^{1}H NMR (500 MHz, $CDCl_3$) δ 7.09 (m, 1H), 7.04 (t, $J = 7.9$ Hz, 1H), 6.84 (dd, $J = 8.0$, 1.6 Hz, 1H), 3.86 (s, 3H), 3.85 (s, 3H), 3.62 (d, $J = 2.7$ Hz, 2H), 2.14 (t, $J = 2.7$ Hz, 1H); ^{13}C NMR (125 MHz, $CDCl_3$) δ 152.6, 146.5, 130.2, 124.0, 121.0. 111.2, 82.2, 69.9, 60.5, 55.8, 19.2; IR (neat, KBr, cm^{-1})

3290, 2937, 1587, 1483, 1273, 1074, 748; HRMS (FAB, M^+) *m/z* 176.0845 (calculated for $C_{11}H_{12}O_2$, 176.0837).

2,4-Diamino-5-[3-(2,3-dimethoxyphenyl)prop-1-ynyl]-6-ethylpyrimidine (22). To an oven-dried 8 mL screw-cap vial was added alkyne **21** (0.145 g, 0.823 mmol), 2,4-diamino-6-ethyl-5-iodopyrimidine (0.108 g, 0.409 mmol), CuI (0.010 g, 0.052 mmol, ~13%), and $Pd(PPh_3)_2Cl_2$ (20 mg, 0.028 mmol, ~7%). Degassed (argon purge) anhydrous DMF (1.0 mL) and triethylamine were added (1.0 mL each), and the mixture was degassed once using the freeze−pump−thaw method. The vial was sealed under argon with a rubber septum and heated at 60 °C for 3 h. After cooling, the orange mixture was diluted with EtOAc (60 mL) and washed with a water/saturated $NaHCO_3$ solution (1:2, 20 mL × 3) and brine (20 mL). The organic phase was dried over sodium sulfate and concentrated to afford the crude product that was purified by flash chromatography (SiO_2 14 g, EtOAc) to afford the still pyrimidine **22** (0.094 g, 73%) as an amber powder. An analytical sample was generated by triturating under ether: TLC $R_f = 0.22$ (EtOAc); mp 158−160 °C; ^{1}H NMR (500 MHz, $CDCl_3$) δ 7.08 (dd, $J = 7.8$, 1.7 Hz, 1H), 7.05 (t, $J = 7.8$ Hz, 1H), 6.85 (dd, $J = 7.8$, 1.7 Hz, 1H), 5.16 (bs, 2H), 4.76 (bs, 2H), 3.89 (s, 2H), 3.88 (s, 6H), 2.69 (q, $J = 7.6$ Hz, 2H), 1.22 (t, $J = 7.6$ Hz, 3H); ^{13}C NMR (125 MHz, $CDCl_3$) δ 173.3, 164.5, 160.7, 152.7, 146.7, 131.0, 124.1, 121.0, 111.3, 96.6, 90.8, 74.9, 60.5, 55.8, 29.6, 20.8, 12.6; HRMS (FAB, MH^+) *m/z* 313.1645 (calculated for $C_{17}H_{21}N_4O_2$, 313.1665); HPLC (a) $t_R = 5.34$ min, 97.7%, (b) $t_R = 9.42$ min, 97.2%.

2,4-Diamino-5-(3-phenylprop-1-ynyl)-6-ethylpyrimidine (24). To an oven-dried 8 mL screw-cap vial was added 2,4-diamino-6-ethyl-5-iodopyrimidine (0.132 g, 0.50mmol), CuI (7.0 mg, 0.035 mmol, 7%), and $Pd(PPh_3)_2Cl_2$ (25.0 mg, 0.035 mmol, 7% Pd). Degassed (argon purge) anhydrous DMF (2.0 mL) was added followed by 3-phenyl-1-propyne **23** (0.087, 0.75 mmol) as a solution in DMF (0.5 mL). Degassed (argon purge) anhydrous triethylamine was added (2.5 mL), and the mixture was degassed once using the freeze−pump−thaw method. The vial was sealed under argon and heated at 50 °C for 8 h, then cooled to room temperature and stirred for another 18 h. After cooling, the orange solution was diluted with EtOAc (20 mL) and washed twice with a water/saturated $NaHCO_3$ solution (1:2, 7.5 mL) and brine 7.5 mL). The organic phase was dried over $MgSO_4$ and concentrated to afford the crude product that was purified by flash chromatography (SiO_2 40 g, 2% MeOH/$CHCl_3$) to afford coupled pyrimidine **24** as a pale solid (78.6 mg, 62%). An analytical sample was obtained by crystallization from MeCN. TLC $R_f = 0.56$ (9:1 $CHCl_3$/MeOH); mp, decomposed above 118.5 °C; ^{1}H NMR (500 MHz, $CDCl_3$) δ 7.42 (d, $J = 8.3$ Hz, 2H), 7.37 (t, $J = 8.3$, 2H Hz), 7.29 (t, $J = 8.3$ Hz,1H), 5.22 (bs, 2H), 4.96 (bs, 2H), 3.92 (s, 2H), 2.72 (q, $J = 6.0$ Hz, 2H), 1.24 (t, $J = 6.0$ Hz, 3H); ^{13}C NMR (125 MHz, $CDCl_3$) δ 173.5, 164.5, 160.8, 136.9, 128.7, 127.8, 126.8, 96.4, 90.5, 75.4, 29.7, 26.2, 12.6; HRMS (FAB, MH^+) *m/z* 253.1461 (calculated for $C_{15}H_{17}N_4$, 253.1453); HPLC (a) $t_R = 5.32$ min, 95.9%, (b) $t_R = 9.18$ min, 95.9%.

Acknowledgment. The authors gratefully acknowledge Justin Fair (University of Connecticut) for his assistance in performing the HPLC analyses and funding from NIAID Grant AI073375.

Supporting Information Available: Details of HPLC purity determinations for compounds **15**−**18**, **20**, **22**, and **24** and instrumentation; tabulated data; copies of chromatograms; ^{1}H NMR and ^{13}C NMR spectra of compounds **13**−**18**, **20**−**22**, and **24** and appropriate intermediates; and elemental analysis data for compounds **15** and **20**. This material is available free of charge via the Internet at http://pubs.acs.org.

References

(1) Mock, M.; Fouet, A. Anthrax. *Annu. Rev. Microbiol.* **2001**, *55*, 647–671.
(2) Coker, P.; Smith, K.; Hugh-Jones, M. Antimicrobial susceptibilities of diverse *Bacillus anthracis* isolates. *Antimicrob. Agents Chemother.* **2002**, *46*, 3843–3845.
(3) Davidson, R.; Cavalcanti, R.; Brunton, J.; Bast, D.; DeAzavedo, J.; Kibsey, P.; Fleming, C.; Low, D. Resistance to levofloxacin and failure of treatment of Pneumococcal pneumonia. *N. Engl. J. Med.* **2002**, *346*, 747–750.
(4) Neuhauser, M.; Weinstein, R.; Rydman, R.; Danziger, L.; Karam, G.; Quinn, J. Antibiotic resistance among gram-negative *Bacilli* in US intensive care units. *JAMA, J. Am. Med. Assoc.* **2003**, *289*, 885–888.
(5) Barrow, E.; Bourne, P.; Barrow, W. Functional cloning of *Bacillus anthracis* dihydrofolate reductase and confirmation of natural resistance to trimethoprim. *Antimicrob. Agents Chemother.* **2004**, *48*, 4643–4649.
(6) Sirotnak, F.; Burchall, J.; Ensminger, W.; Montgomery, J. *Folate Antagonists as Therapeutic Agents*; Academic Press: New York, 1984.
(7) Fleming, G.; Schilsky, R. Antifolates: the next generation. *Semin. Oncol.* **1992**, *19*, 707–719.
(8) Salter, A. Trimethoprim-sulfamethoxazole: an assessment of more than 12 years of use. *Rev. Infect. Dis.* **1982**, *4*, 196–236.
(9) Roth, B.; Rauckman, B.; Ferone, R.; Baccanari, D.; Champness, J.; Hyde, R. 2,4-Diamino-5-benzylpyrimidines as antibacterial agents. 7. Analysis of the effect of 3,5-dialkyl substituent size and shape on binding to four different dihydrofolate reductase enzymes. *J. Med. Chem.* **1987**, *30*, 348–356.
(10) Plowe, C.; Kublin, J.; Dzinjalamala, F. K.; Kamwendo, D.; Mukadam, R.; Chimpeni, P.; Molyneux, M.; Taylor, T.; Terrie, E. Sustained efficacy of sulfadoxine-pyrimethamine for uncomplicated falciparum malaria in Malawi after 10 years as first-line treatment: five-year prospective study. *Br. Med. J.* **2004**, *328*, 545–8.
(11) Armstrong, C.; Smith, C. Cyclization and N-dealkylation of chloroguanide by rabbit and rat hepatic microsomes. *Toxicol. Appl. Pharmacol.* **1974**, *29*, 90.
(12) Rosowsky, A.; Forsch, R.; Queener, S. Further studies on 2,4-diamino-5-(2′,5′-disubstituted benzyl)pyrimidines as potent and selective inhibitors of dihydrofolate reductases from three major opportunistic pathogens of AIDS. *J. Med. Chem.* **2003**, *46*, 1726–1736.
(13) Bertino, J. Karnofsky memorial lecture: ode to methotrexate. *J. Clin. Oncol.* **1993**, *11*, 5–14.
(14) Joska, T.; Anderson, A. Structure−activity relationships of *Bacillus cereus* and *Bacillus anthracis* dihydrofolate reductase: toward the identification of new potent drug leads. *Antimicrob. Agents Chemother.* **2006**, *50*, 3435–3443.
(15) Bennett, B.; Xu, H.; Simmerman, R.; Lee, R.; Dealwis, C. Crystal structure of the anthrax drug target *Bacillus anthracis* dihydrofolate reductase. *J. Med. Chem.* **2007**, *50*, 4374–4381.
(16) Pelphrey, P.; Popov, V.; Joska, T.; Beierlein, J.; Bolstad, E.; Fillingham, Y.; Wright, D.; Anderson, A. Highly efficient ligands for DHFR from *Cryptosporidium hominis* and *Toxoplasma gondii* inspired by structural analysis. *J. Med. Chem.* **2007**, *50*, 940–950.
(17) Chan, D.; Anderson, A. Towards species-specific antifolates. *Curr. Med. Chem.* **2006**, *13*, 377–398.
(18) Bates, P.; Kelley, L.; MacCallum, R.; Sternberg, M. Enhancement of protein modeling by human intervention in applying the automatic programs 3D-JIGSAW and 3D-PSSM. *Proteins* **2001**, *45* (S5), 39–46.
(19) Anderson, A. Two crystal structures of dihydrofolate reductase-thymidylate synthase from *Cryptosporidium hominis* reveal protein: ligand interactions including a structural basis for observed antifolate resistance. *Acta Crystallogr.* **2005**, *F61*, 258–262.
(20) Bolin, J.; Filman, D.; Matthews, D.; Hamlin, R.; Kraut, J. Crystal structures of *Escherichia coli* and *Lactobacillus casei* dihydrofolate reductase refined at 1.7 Å resolution. I. General features and binding of methotrexate. *J. Biol. Chem.* **1982**, *257*, 13650–13662.
(21) Cody, V.; Schwalbe, C. Structural characteristics of antifolate dihydrofolate reductase enzyme interactions. *Crystallogr. Rev.* **2006**, *12*, 301–333.
(22) Yuvaniyama, J.; Chitnumsub, P.; Kamchonwongpaisan, S.; Vanichtanankul, J.; Sirawaraporn, W.; Taylor, P.; Walkinshaw, M.; Yuthavong, Y. Insights into antifolate resistance from malarial DHFR-TS structures. *Nat. Struct. Biol.* **2003**, *10*, 357–365.
(23) Richardson, M. L.; Stevens, M. F. G. Structural studies on bioactive compounds. Part 37. Suzuki coupling of diaminopyrimidines: a new synthesis of the antimalarial drug pyrimethamine. *J. Chem. Res., Synop.* **2002**, *10*, 482.
(24) Roth, B.; Aig, E.; Lane, K.; Rauckman, B. S. 2,4-Diamino-5-benzylpyrimidines as antibacterial agents. 4. 6-Substituted trimethoprim derivatives from phenolic Mannich intermediates. Application to the synthesis of trimethoprim and 3,5-dialkylbenzyl analogs. *J. Med. Chem.* **1980**, *23* (5), 535–541.

JM800776A